Potential of off-gas analyses for sequentially operated reactors demonstrated on full-scale aerobic granular sludge technology

Baeten, Janis E.; van Dijk, Edward J.H.; Pronk, Mario; van Loosdrecht, Mark C.M.; Volcke, Eveline I.P.

DOI
10.1016/j.scitotenv.2021.147651

Publication date
2021

Document Version
Final published version

Published in
Science of the Total Environment

Science of the Total Environment 787 (2021) 147651

Contents lists available at ScienceDirect

Science of the Total Environment

journal homepage: www.elsevier.com/locate/scitotenv

Potential of off-gas analyses for sequentially operated reactors demonstrated on full-scale aerobic granular sludge technology

Janis E. Baeten [a], Edward J.H. van Dijk [b,c], Mario Pronk [b,c], Mark C.M. van Loosdrecht [b], Eveline I.P. Volcke [a,*]

[a] BioCo Research Group, Department of Green Chemistry and Technology, Coupure Links 653, 9000 Gent, Ghent University, Belgium
[b] Environmental Biotechnology, Department of Biotechnology, Delft University of Technology, Van der Maasweg 9, 2629 HZ Delft, the Netherlands
[c] Royal HaskoningDHV, Laan 1914 35, Amersfoort 3800, AL, the Netherlands

HIGHLIGHTS

- Off-gas measurements were performed on a full-scale aerobic granular sludge reactor.
- Derivation of multiple variables with a single off-gas sampler is demonstrated.
- Liquid-gas transfer, aeration characteristics and greenhouse gas emissions are derived.
- Concentrations, conversion rates, influent TOC & N and sludge production are derived.
- There is untapped potential of off-gas analyses for sequentially operated reactors.

GRAPHICAL ABSTRACT

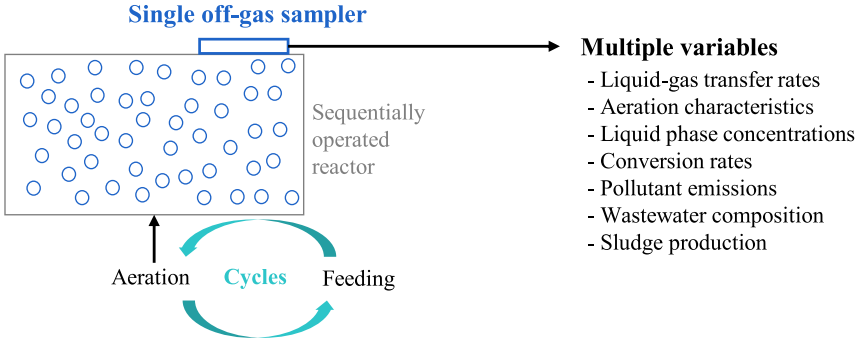

ARTICLE INFO

Article history:
Received 15 March 2021
Received in revised form 22 April 2021
Accepted 5 May 2021
Available online 8 May 2021

Editor: Yifeng Zhang

Keywords:
Sequencing batch reactor
Floating hood
Aeration
Mass balance
Emission
Absorption

ABSTRACT

This work shows how more variables can be monitored with a single off-gas sampler on sequentially operated than on continuously fed and aerated reactors and applies the methods to data from a full-scale aerobic granular sludge reactor as a demonstration and to obtain insight in this technology. First, liquid-gas transfer rates were calculated. Oxygen (O_2) absorption and carbon dioxide (CO_2) emission rates showed comparable cyclic trends due to the coupling of O_2 consumption and CO_2 production. Methane (CH_4) emissions showed a stripping profile and nitrous oxide (N_2O) emissions showed two peaks each cycle, which were attributed to different production pathways. Secondly, aeration characteristics were calculated, of which the gradual improvement within cycles was explained by surfactants degradation. Thirdly, liquid phase concentrations were estimated from off-gas measurements via a novel calculation procedure. As such, an average influent CH_4 concentration of 0.7 $g \cdot m^{-3}$ was found. Fourthly, reaction rates could be estimated from off-gas data because no feeding or discharge occurred during reaction phases. The O_2 consumption rate increased with increasing dissolved oxygen and decreased once nitrification was complete. Fifthly, greenhouse gas emissions could be derived, indicating a 0.06% N_2O emission factor. Sixthly, off-gas gave an indication of influent characteristics. The CO_2 emitted per kg COD catabolized corresponded with the TOC/COD ratio of typical wastewater organics in cycles with balanced nitrification and denitrification. High nitrogen removal efficiencies were associated with high catabolized COD/N ratios as estimated from the O_2 absorption. Finally, mass balances could be closed using off-gas O_2 data. As such, an observed yield of 0.27 g COD/g COD was found. All these variables could be estimated with a single sampler because aeration

* Corresponding author.
E-mail addresses: Janis.Baeten@UGent.be (J.E. Baeten), Edward.van.Dijk@rhdhv.com (E.J.H. van Dijk), Mario.Pronk@rhdhv.com (M. Pronk), M.C.M.vanLoosdrecht@tudelft.nl (M.C.M. van Loosdrecht), Eveline.Volcke@UGent.be (E.I.P. Volcke).

https://doi.org/10.1016/j.scitotenv.2021.147651

without feeding creates a more homogeneous off-gas composition and simplifies liquid-phase mass balances. Therefore, off-gas analyzers may have a broader application potential for sequentially operated reactors than currently acknowledged.

1. Introduction

The chemical composition of the gas leaving an aerobic wastewater treatment reactor reflects the liquid-gas transfer of its constituents, such as oxygen (O_2), carbon dioxide (CO_2), nitrous oxide (N_2O), nitric oxide (NO), volatile organic compounds (VOC), methane (CH_4) etc. The liquid-gas transfer is in turn affected by the (biological) consumption or production of these substances and their presence in the influent. For example, oxygen is consumed and thus the off-gas contains less oxygen than the aeration air. In contrast, the carbon dioxide content will be higher in the off-gas, because it is produced during heterotrophic growth (Hellinga et al., 1996). Also methane is often enriched in the off-gas, as it enters via the influent (Daelman et al., 2012). Due to this relationship between the gas composition and processes in the water, off-gas analyses can be used for monitoring and control. Moreover, such analyses have advantages compared to measurements in the liquid phase: no chemical reagents are required, a gas sample is well mixed and has been in contact with a large volume of water and maintenance is minimal due to the limited fouling and corrosive effects of the gas (Hellinga et al., 1996; Sonnleitner, 2013; Mears et al., 2017; Vanrolleghem and Lee, 2003).

Off-gas analyses have been used in many studies, but gas samplers and analyzers are not (yet) part of the typical instrumentation on wastewater treatment plants. Full-scale measurements have primarily been used to calculate aeration characteristics (Table 1), as aeration is a major cost factor (Rosso and Stenstrom, 2005). For example, Gillot and Heduit (2000) used the oxygen content in the off-gas to calculate the Oxygen Transfer Efficiency (OTE). The liquid-gas transfer rate of different substances from full-scale installations can also be monitored, based on measured off-gas concentrations and flow rates. For example, Leu et al. (2010) tracked the oxygen and carbon dioxide transfer rate over time to detect ammonium breakthrough periods. Finally, cumulative emissions over a longer period (hours to years) have been calculated for different pollutants, e.g. VOCs (Sree et al., 2000) or nitrous oxide and methane (Daelman et al., 2013a). Only a few studies have derived other key variables from off-gas analyses, such as liquid-phase concentrations, conversion rates, influent characteristics and amounts of sludge produced, even though this is possible (Table 1). This indicates that the potential of off-gas analyses is under-recognized.

One reason for the limited use of off-gas data is that representative gas sampling and the calculation of key variables are challenging for reactors with continuous aeration, feeding and discharge, while this reactor type is widespread (Table 1). Representative sampling is complicated due to the simultaneous reactions and water flows, which produce spatial concentration gradients in the liquid phase along the flow direction (Vanrolleghem et al., 2003; Meijer et al., 2001), causing a heterogeneous off-gas composition in turn (Rosso et al., 2011; Amerlinck et al., 2016; Caniani et al., 2019) (Fig. 1). Therefore, a floating hood is often successively placed at different locations or several hoods are used simultaneously (Table 1). Only some full-scale reactors are completely covered, which makes sampling easier (Daelman et al., 2013a; Winter et al., 2012; Mampaey et al., 2016). Also the calculation of a consumption rate of a substance i ($\dot{R}_i^L$, in $g \cdot min^{-1}$) from mass balances is difficult in continuous reactors (Eq. (1)), as it does not only require the knowledge of the liquid-gas transfer rate ($\dot{m}_i^{L\text{-}G}$, in $g \cdot min^{-1}$) and a continuous measurement of the liquid phase concentration (C_i^L, in $g \cdot m^{-3}$), but also the incoming and outgoing liquid phase mass flow rates ($\dot{m}_{in,i}^L$ and $\dot{m}_{out,i}^L$, respectively, in $g \cdot min^{-1}$, through the liquid volume V^L, in m^3) should be known (Chiesa et al., 1990; ASCE, 1997).

Simultaneous feeding and aeration :

$$\frac{dC_i^L V^L}{dt} = \left(\dot{m}_{in,i}^L - \dot{m}_{out,i}^L\right) - \dot{m}_i^{L-G}(t) - \dot{R}_i^L(t) \quad (1)$$

To estimate consumption rates in continuously operated systems, several methods have been developed in literature to estimate the missing terms in Eq. (1), which all require simplifying assumptions that are not generally applicable, additional off-line measurements or extensive models and this could discourage their widespread adoption. For example, the calculation of the oxygen consumption rate by Rieth et al. (1995) and Rosso et al. (2011) relied on a negligible accumulation term. To estimate the carbon dioxide production rate, Weissenbacher et al. (2007) relied on daily off-line measurements of the inorganic carbon in the reactor and influent. Leu et al. (2009, 2010) used off-gas oxygen and carbon dioxide data to calibrate and validate a bioconversion model based on the activated sludge models (ASM) (Henze et al., 2000), which was used in turn to estimate the nitrification and heterotrophic conversion rates.

Off-gas analyses may be more practically applicable in case of sequentially operated reactors. When aeration occurs without simultaneous feeding or discharge, the liquid phase shows no significant spatial concentration gradients in the horizontal direction (Ronner-Holm et al., 2006; Lindblom et al., 2016; Ni et al., 2009; Keller and Yuan, 2002). Therefore, also the off-gas composition is more homogeneous and a single off-gas sampler is more representative for the complete reactor (Fig. 1). Besides, the absence of feeding during aerated phases allows easier and more accurate rate estimations from mass balances (Eq. (2)), as liquid phase mass flow rates are absent.

Separated feeding and aeration : $$\frac{dC_i^L V^L}{dt} = -\dot{m}_i^{L-G}(t) - \dot{R}_i^L(t) \quad (2)$$

Such reactors can thus be used as a large respirometer (Yoong et al., 2000; Spanjers et al., 1996).

Even though sequentially operated reactors have traditionally been applied less frequently on full-scale (Kent et al., 2018) (Table 1), they are gaining ground through the installation of aerobic granular sludge reactors, which rely on separate feeding and aeration phases. Aerobic granular sludge reactors have become very popular due to the associated savings in space and energy (Pronk et al., 2017). This is an extra incentive to revaluate the potential of off-gas for monitoring and control.

In this contribution, the full potential of off-gas analyses for sequentially operated reactors is demonstrated by simultaneously deriving all the types of key variables with a single sampler and without requiring bioconversion models or additional off-line liquid-phase analyses (Table 1). It is also the first full-scale off-gas monitoring campaign published in scientific literature on aerobic granular sludge. After the methodology, the dynamics of the liquid-gas transfer rates of oxygen, carbon dioxide, nitrous oxide and methane within a cycle are linked to processes occurring in the liquid phase. Then aeration characteristics, liquid phase concentrations and conversion rates are derived. Next, the cumulative amounts transferred over one or more cycles are used to estimate greenhouse gas emissions and wastewater characteristics and the sludge production is estimated via a mass balance. Finally, perspectives for practical applications are provided.

Table 1
Journal publications using continuous measurements of the off-gas composition from operational aerobic wastewater treatment reactors. An "x" indicates which types of variables were derived in each study. Strictly controlled lab-scale systems designed for studying reaction kinetics are not included (Gapes and Keller, 2001; Gapes et al., 2003).

Reference	Scale	Multiple sampling points	Operation	Sludge	Liquid-gas transfer rates	Aeration characteristics	Liquid-phase concentrations	Conversion rates	Pollutant emissions	Wastewater composition	Sludge production
Shiskowski and Mavinic (2005)	Lab		Continuous	Flocculent							
Wu et al. (2015)	Lab		Continuous	Flocculent							
Spérandio and Paul (1997)	Lab		Sequential	Flocculent	x			x			
Kong et al. (2013)	Lab		Sequential	Granular	x				x		
Lochmatter et al. (2014)	Lab		Sequential	Granular					x		
Guimarães et al. (2017)	Lab		Sequential	Granular					x		
Velho et al. (2017)	Lab		Sequential	Granular					x		
Rieth et al. (1995)	Pilot		Continuous	Flocculent		x		x			
Sree et al. (2000)	Pilot		Continuous	Flocculent	x				x		
Weissenbacher et al. (2007)	Pilot		Continuous	Flocculent	x		x	x			
Butler et al. (2009)	Pilot		Continuous	Flocculent							
Cecconi et al. (2019)	Pilot		Sequential	Granular	x	x		x			
Redmon et al. (1983)	Full	x	Continuous	Flocculent		x					
Groves et al. (1992)	Full	x	Continuous	Flocculent		x					
Gillot and Heduit (2000)	Full	x	Continuous	Flocculent		x					
Makinia and Wells (2000)	Full	x	Continuous	Flocculent		x					
Mueller et al. (2000)	Full	x	Continuous	Flocculent	x	x					
Sahlmann et al. (2004)	Full	x	Continuous	Flocculent	x	x					
Rosso et al. (2005)	Full	x	Continuous	Flocculent		x					
Schuchardt et al. (2007)	Full	x	Continuous	Flocculent	x	x					
Gillot and Heduit (2008)	Full	NA	Continuous	Flocculent		x					
Leu et al. (2009)	Full	x	Continuous	Flocculent	x	x		x		x	
Leu et al. (2010)	Full	x	Continuous	Flocculent	x	x		x			
Sandberg (2010)	Full		Continuous	Flocculent		x					
Racault et al. (2011)	Full	NA	Continuous	Flocculent		x					
Rosso et al. (2011)	Full	x	Continuous	Flocculent & biofilm	x	x		x			
Winter et al. (2012)	Full		Continuous	Flocculent	x				x		
Daelman et al. (2013a)	Full		Continuous	Flocculent	x				x		
Amerlinck et al. (2016)	Full	x	Continuous	Flocculent		x					
Mampaey et al. (2016)	Full		Continuous	Flocculent	x	x	x	x	x		x
Caivano et al. (2017)	Full	x	Continuous	Flocculent		x			x		
Bellandi et al. (2018)	Full	x	Continuous	Flocculent	x				x		
Spinelli et al. (2018)	Full	x	Continuous	Flocculent	x				x		
Caniani et al. (2019)	Full	x	Continuous	Flocculent					x		
Aviles et al. (2020)	Full	x	Continuous	Flocculent		x					
This study	Full		Sequential	Granular	x	x	x	x	x	x	x

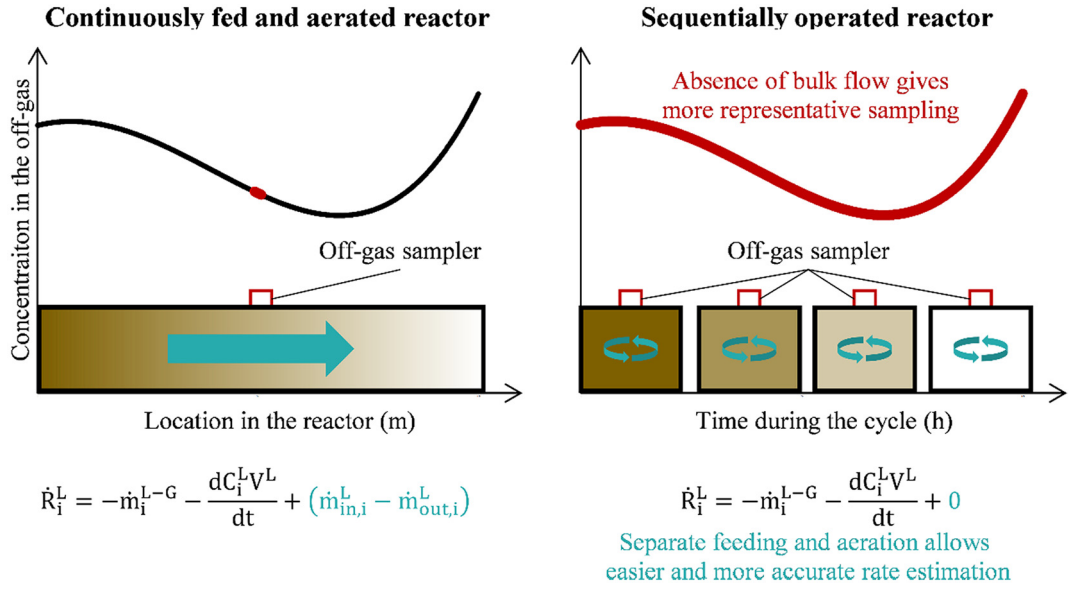

Fig. 1. Conceptual difference between off-gas analysis with a single sampler on a continuously fed and aerated (left) and a sequentially operated reactor during the aeration phase (right).

2. Materials and methods

2.1. Process under study

A four and a half day monitoring campaign was performed from 31 July to 4 August 2017 at one of the three Nereda® aerobic granular sludge reactors at the municipal wastewater treatment plant in Dinxperlo (NL) of the water board Rijn en IJssel. Nereda® is a registered trademark for a proprietary aerobic granular sludge technology owned by Royal HaskoningDHV. On average, the plant treats 3370 $m^3 \cdot d^{-1}$ with respective concentrations of organics, total nitrogen and total phosphorus of 538 g COD$\cdot m^{-3}$, 48 g N$\cdot m^{-3}$ and 7 g P$\cdot m^{-3}$ in 2017 (Fig. S5 in the Supplementary information shows the liquid phase nitrate/nitrite, ammonium and phosphorus concentrations during the monitoring campaign in particular). The total suspended solids in the mixed liquor constituted 11 g TSS$\cdot L^{-1}$ at the time of the measurements, of which 84% had a diameter above 0.2 mm. The bottom of the 1250 m^3 reactor (7.35 m water depth and 170 m^2 surface) was covered with fine-bubble diffusers.

A typical dry weather cycle of the reactor takes about 5.5 h (Fig. 3). First, simultaneous upward feeding and discharge takes place without aeration for 1 h. Next, the water level is decreased from about 7.5 to 7.35 m during a twenty minute period to compensate for the gas hold-up during the subsequent 3.5-hour reaction phase. The reaction phases start with a period with strong and continuous aeration to favour nitrification in particular. Once the ammonium concentration reaches its set-point, weaker, intermittent aeration is used to stimulate denitrification of the accumulated nitrate while keeping reactor contents mixed. The cycle ends with a 45-minute period during which settling and sludge withdrawal occurs. The cycle length and influent volume per batch are automatically adapted to the hydraulic and pollutant load conditions. Phosphorus is mainly removed biologically during the reaction period, but iron chloride is dosed inside the reactor or in the sand bed afterwards to complement the biological phosphorus removal when necessary.

2.2. Measured variables and data treatment

2.2.1. Off-gas and liquid phase measurements

A floating hood covering an area of 0.55 m^2 was used to collect off-gas from the water surface (Fig. S1). The dead volume inside the hood was reduced with polyurethane foam, until about 0.1 m^3 remained when floating (Fig. S2). Off-gas was sampled from the hood and sent through a cooler to dry before entering an on-line analyzer to measure the mole fractions of oxygen, carbon dioxide (NGA 2000 MLT1, Rosemount, Emerson), methane and nitrous oxide (Xentra Continuous Emission Analyzer 4900, Servomex). The on-site atmosphere was analyzed for 5 min every hour (Fig. S3). The atmospheric temperature, pressure and relative humidity were monitored (Bosch BME280).

Standard on-line monitoring data were used to supplement the off-gas analysis. The reactor temperature, dissolved oxygen (LDO, Hach), ammonium (Amtax, Hach), nitrate plus nitrite (Nitratax, Hach) and phosphate concentration (Phosphax, Hach) were measured in-situ. The rotational speed of the three positive displacement blowers (Aerzen Blower Delta Hybrid/D12S), the position of the valves between the blowers and the air diffusers and the influent flow rate were logged.

2.2.2. Gas flow rates

The volumetric air flow rate into the reactor Q_{in}^G ($m^3 \cdot min^{-1}$ expressed under atmospheric temperature and pressure) was calculated from the frequency of rotation of the three blowers, using specifications provided by the supplier, and from the opening and closing of the valves (Fig. 2). To calculate the off-gas flow rate Q_{out}^G ($m^3 \cdot min^{-1}$), this intake flow rate Q_{in}^G was corrected for the temperature difference between the atmosphere T_{air}^G (K) and off-gas via Charles' law (Eq. (3)).

$$Q_{out}^G(t) = Q_{in}^G(t) \cdot \frac{T_{reactor}^L(t)}{T_{air}^G(t)} \quad (3)$$

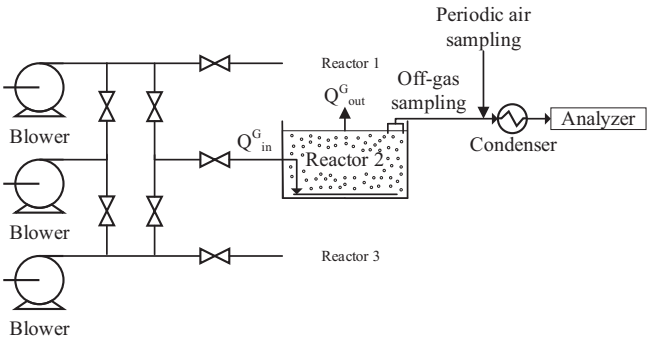

Fig. 2. Simplified scheme of the gas flows at the plant.

The off-gas temperature was assumed equal to that of the reactor $T^L_{reactor}$ (K), given the fine bubbles and high water column over which thermal equilibrium can develop. Changes in the total molar flow rate due to net absorption or stripping were neglected. This is a common assumption (Redmon et al., 1983; Le et al., 2016) and it is also justified in this particular case, as the nitrogen production calculated via the measured amount of denitrification during the monitoring period accounted to only 0.3 vol% of the aeration air.

2.2.3. Conversion of gas phase mole fractions to concentrations

Gas phase mole fractions x^G_i ($mole \cdot mole^{-1}$) were converted to concentrations C^G_i ($g \cdot m^{-3}$) through the ideal gas law (Eq. (4)).

$$C^G_i(t) = x^G_i(t) \cdot \frac{p^G_{air}(t) \cdot M_i}{R \cdot T^G(t)} \quad (4)$$

where p^G_{air} (Pa) denotes the measured atmospheric pressure, M_i ($g \cdot mole^{-1}$) the molecular mass of substance i, R (8.314 $J \cdot mole^{-1} \cdot K^{-1}$) the ideal gas constant, and T^G (K) the temperature of the gas, where the measured atmospheric temperature T^G_{air} was used to obtain the atmospheric concentrations $C^G_{in,i}$ ($g \cdot m^{-3}$), while the measured reactor temperature $T^L_{reactor}$ was used for the off-gas concentrations $C^G_{out,i}$ ($g \cdot m^{-3}$).

The mole fractions x^G_i in Eq. (4) were derived from the measured values $x^G_{measured,i}$ after several corrections (Eq. (5)).

$$x^G_i(t) = x^G_{measured,i}(t+\tau) \cdot \frac{p^G_{air,cal}}{p^G_{air}(t)} \cdot \left(1 - RH^G(t) \cdot \frac{133.322 \cdot 10^{8.0727 - \frac{1732.32}{T^G(t) - 39.466}}}{p^G_{air}(t)}\right) \quad (5)$$

A pure time delay τ (min) of 3 min was used for the off-gas, to make the drop in the oxygen content coincide with the start of aeration phases. This delay originates from the residence time of gas in the reactor and tubing. No time delay was used for the atmospheric sampling because of the short tubing. Secondly, the pressure ratio was introduced in Eq. (5) to undo the fluctuations of the signal (Fig. S4) by compression or decompression inside the analyzer when the atmospheric pressure p^G_{air} deviated from the value during calibration $p^G_{air,cal}$ (Pa). The third factor corrects for the water vapour that condensed in the cooler before analysis, using the relative humidity in the sampled gas RH^G (−) and the equilibrium water content calculated with the Antoine equation (Shriver and Drezdzon, 1986). The reactor temperature and 100% relative humidity were used for the off-gas, as suggested by Redmon et al. (1983), whereas the measured atmospheric temperature and relative humidity were used for the atmosphere. Finally, the missing mole fraction data for the off-gas during sampling of the atmosphere and vice versa were filled up by linear interpolation.

2.3. Calculation of key variables from off-gas analyses

2.3.1. Liquid-gas transfer rates

The liquid-gas transfer rates of O_2, CO_2, CH_4 and N_2O were calculated based on Eq. (6), expressing the liquid-gas transfer rate of a substance i, $\dot{m}^{L-G}_i$ ($g \cdot min^{-1}$) as the difference between the mass flow out of and into the reactor via the gas phase (Eq. (6)) (Baeten et al., 2020).

$$\dot{m}^{L-G}_i(t) = Q^G_{out}(t) \cdot C^G_{out,i}(t) - Q^G_{in}(t) \cdot C^G_{in,i}(t) \quad (6)$$

Eq. (6) implies that the measured off-gas concentrations are representative for the complete reactor surface and that the gas phase is in pseudo steady-state. The former was motivated in this study by the intense mixing during the aeration phases; the latter was fulfilled because of the short residence time of the gas in the reactor, relative to the interphase mass transfer and biological conversion rates (Baeten et al., 2020). Positive liquid-gas transfer rates $\dot{m}^{L-G}_i$ denote a stripping/emission rate. If it is negative, the sign can be reversed to obtain an absorption rate.

2.3.2. Aeration characteristics

The overall volumetric liquid-gas transfer coefficient of a substance i, K_La_i (d^{-1}) can be estimated from its liquid-gas transfer rate $\dot{m}^{L-G}_i$ (Eq. (6)), its liquid phase concentration C^L_i and the reactor volume V^L via Eq. (7) (Henze et al., 2008).

$$K_La_i = \frac{\dot{m}^{L-G}_i(t)}{V^L \cdot \left(C^L_i - C^L_{eq,i}(t)\right)} \quad (7)$$

The calculation of the liquid-gas transfer coefficient K_La_i through Eq. (7) requires measured liquid phase concentrations of substance i. The dissolved oxygen concentrations measurement in this study thus allowed the calculation of the liquid-gas transfer coefficient for oxygen, K_La_{O2}. The equilibrium liquid-phase concentration $C^L_{eq,i}$ ($g \cdot m^{-3}$) in Eq. (7) was calculated (Eq. (8)) via the Henry coefficient h_i ($g \cdot m^{-3}$ in the liquid per $g \cdot m^{-3}$ in the gas) corrected for the reactor temperature (Table 1S), the mean of the mole fraction in the atmosphere and the off-gas $x^G_{mean,i}$ (Eq. (9)) and the mean hydrostatic pressure p^G_{mean} (Eq. (10)) (Baeten et al., 2020).

$$C^L_{eq,i}(t) = h_i(t) \cdot x^G_{mean,i}(t) \cdot \frac{p^G_{mean}(t) \cdot M_i}{R \cdot T^L_{reactor}(t)} \quad (8)$$

$$x^G_{mean,i}(t) = \frac{x^G_{out,i}(t) + x^G_{in,i}(t)}{2} \quad (9)$$

$$p^G_{mean}(t) = p^G_{air}(t) + \rho \cdot g \cdot \frac{H}{2} \quad (10)$$

with ρ ($kg \cdot m^{-3}$) the density of the wastewater, g ($m \cdot s^{-2}$) the gravitational acceleration and H (m) the water height.

For CH_4 and N_2O, no on-line liquid phase measurements were available, so their liquid-gas transfer coefficients K_La_i were derived from the relationship with K_La_{O2} (Eq. (11)) (heyder et al., 1997), using diffusion coefficients D_i ($cm^2 \cdot s^{-1}$) from literature (Table 1S).

$$K_La_i(t) = K_La_{O2}(t) \cdot \sqrt{\frac{D_i}{D_{O2}}} \quad (11)$$

Note that these K_La_i's are calculated under process conditions and are therefore affected by fouling of the diffusers and dissolved substances in the wastewater that hinder liquid-gas transfer (often characterised by the alfa-factor).

Additional aeration characteristics were calculated, namely the (specific standard) oxygen transfer efficiency and the average aeration efficiency. The oxygen transfer efficiency OTE (−) is the fraction of the injected oxygen mass flow that was absorbed by the liquid phase (Eq. (12)) (Henze et al., 2008)

$$OTE(t) = \frac{\dot{m}^{G-L}_{O2}(t)}{Q^G_{in}(t) \cdot C^G_{in,O2}(t)} \quad (12)$$

based on the measured incoming air flow rate, incoming oxygen gas phase concentration and calculated oxygen liquid-gas transfer rate (Eq. (6)). The specific standard oxygen transfer efficiency SSOTE was obtained from Eq. (13), by correcting the OTE for the water depth H and dissolved oxygen concentration and expressing it at a standard temperature and pressure $T^L_{std} = 20$ °C and $p^G_{std} = 1013$ hPa (Gillot et al., 2005a,b).

$$SSOTE(t) = \frac{OTE(t)}{H} \frac{C^L_{eq,i}\left(T^L_{std}, p^G_{std}\right)}{C^L_{eq,i}(t) - C^L_{O2}(t)} 1.024^{\left(20 - T^L_{reactor}(t)\right)} \quad (13)$$

The average aeration efficiency AE ($g\ O_2 \cdot Wh^{-1}$) was calculated according to Eq. (14) (Henze et al., 2008).

$$AE = \frac{m_{O2}^{G-L}}{W} \tag{14}$$

where m_{O2}^{G-L} ($g\ O_2$) represents the total amount of oxygen absorbed during the monitoring campaign, obtained by integration of the liquid-gas transfer rate $\dot{m}_{O2}^{L-G}$ (Eq. (6)). The total work required for aeration W (kWh) was calculated via integration of the power (kW) needed at the rotor shaft, using blower specifications.

2.3.3. Liquid phase concentrations

By rearranging the liquid-gas transfer model from Eqs. (7) to (15), the liquid phase concentration of a substance i can be calculated from its liquid-gas transfer rate $\dot{m}_i^{L-G}$ (Eq. (6)) and the estimated liquid-gas transfer coefficient K_La_i (Eq. (11)).

$$C_i^L(t) = \frac{\dot{m}_i^{L-G}(t)}{K_La_i(t) \cdot V^L} + C_{eq,i}^L(t) \tag{15}$$

Note that the liquid phase concentration of any substance i can be derived from its gas phase concentration through Eq. (15), as long as the gas and liquid phase concentration of oxygen are measured simultaneously, because estimation of K_La_i (Eq. (11)) relies on the value of K_La_{O2} (Eq. (7)).

2.3.4. Conversion rates

The oxygen consumption rate in the liquid phase $\dot{R}_{O2}^L$ ($g \cdot min^{-1}$) was estimated from its absorption rate $\dot{m}_{O2}^{G-L}$ ($g \cdot min^{-1}$, Eq. (6)) via a liquid-phase mass balance (Eq. (1)), in which the accumulation term was calculated through a central difference approximation (Eq. (16)) with $\Delta t = 0.5$ min.

$$\dot{R}_{O2}^L(t) = \dot{m}_{O2}^{G-L}(t) - \frac{C_{O2}^L(t+\Delta t) - C_{O2}^L(t-\Delta t)}{2\Delta t} \cdot V^L \tag{16}$$

2.3.5. Sludge production and N and COD conversion via mass balances

From the liquid phase mass balances of oxygen, COD, nitrogen and nitrate over the complete monitoring period, the following unmeasured variables were derived (see Supplementary information 1.3): the COD mass incorporated in sludge (R_{COD}^{sludge}, in g COD, Eq. (17)), the COD mass consumed catabolically via aerobic conversion ($R_{aer,COD}^L$, in g COD, Eq. (18)), the nitrogen mass nitrified ($R_{nit,N}^L$, in g N, Eq. (19)) and the nitrogen mass denitrified ($R_{den,N}^L$, in g N, Eq. (20)).

$$R_{COD}^{sludge} = -0.893 m_{O2}^{G-L} + 0.893\left(m_{in,COD}^L - m_{out,COD}^L\right) + 1.53\left(m_{in,N}^L - m_{out,N}^L\right) + 4.08 m_{out,NO3}^L \tag{17}$$

$$R_{aer,COD}^L = 0.714 m_{O2}^{G-L} + 0.286\left(m_{in,COD}^L - m_{out,COD}^L\right) - 4.08\left(m_{in,N}^L - m_{out,N}^L\right) - 3.26 m_{out,NO3}^L \tag{18}$$

$$R_{nit,N}^L = 0.0625 m_{O2}^{G-L} - 0.0625\left(m_{in,COD}^L - m_{out,COD}^L\right) + 0.893\left(m_{in,N}^L - m_{out,N}^L\right) + 0.714 m_{out,NO3}^L \tag{19}$$

$$R_{den,N}^L = 0.0625 m_{O2}^{G-L} - 0.0625\left(m_{in,COD}^L - m_{out,COD}^L\right) + 0.893\left(m_{in,N}^L - m_{out,N}^L\right) - 0.286 m_{out,NO3}^L \tag{20}$$

In these expressions, m_{O2}^{G-L} ($g\ O_2$) is the total amount of absorbed oxygen derived via the off-gas analyses. The amount of COD and nitrogen entering and leaving the reactor via the liquid phase $m_{in,COD}^L$ (g COD), $m_{out,COD}^L$ (g COD), $m_{in,N}^L$ (g N) and $m_{out,N}^L$ (g N) and the nitrate in the effluent $m_{out,NO3}^L$ (g N) were derived from the historical average influent and effluent concentrations. Due to the sequential reactor operation, the net ammonium and nitrate mass removed over the monitoring period could also be calculated via the on-line ammonium and nitrite/nitrate measurements (Fig. 3). The mass of ammonium removed during every cycle j, $R_{NH4,j}^L$ (g N), was estimated from the decrease of the ammonium concentration during the reaction phase from $C_{NH4,start\ reaction\ j}^L$ to $C_{NH4,end\ reaction\ j}^L$ (Eq. (21)).

$$R_{NH4,j}^L = \left[C_{NH4,start\ reaction\ j}^L - C_{NH4,end\ reaction\ j}^L\right] \cdot V^L \tag{21}$$

The nitrate removal during cycle j, $R_{NO3,j}^L$ (g N), was estimated as the sum of the nitrogen removal during the reaction phase and the residual denitrification during the other phases (van Dijk et al., 2018). During the reaction phase, the nitrogen removal $R_{NO3,reaction\ j}^L$ was calculated

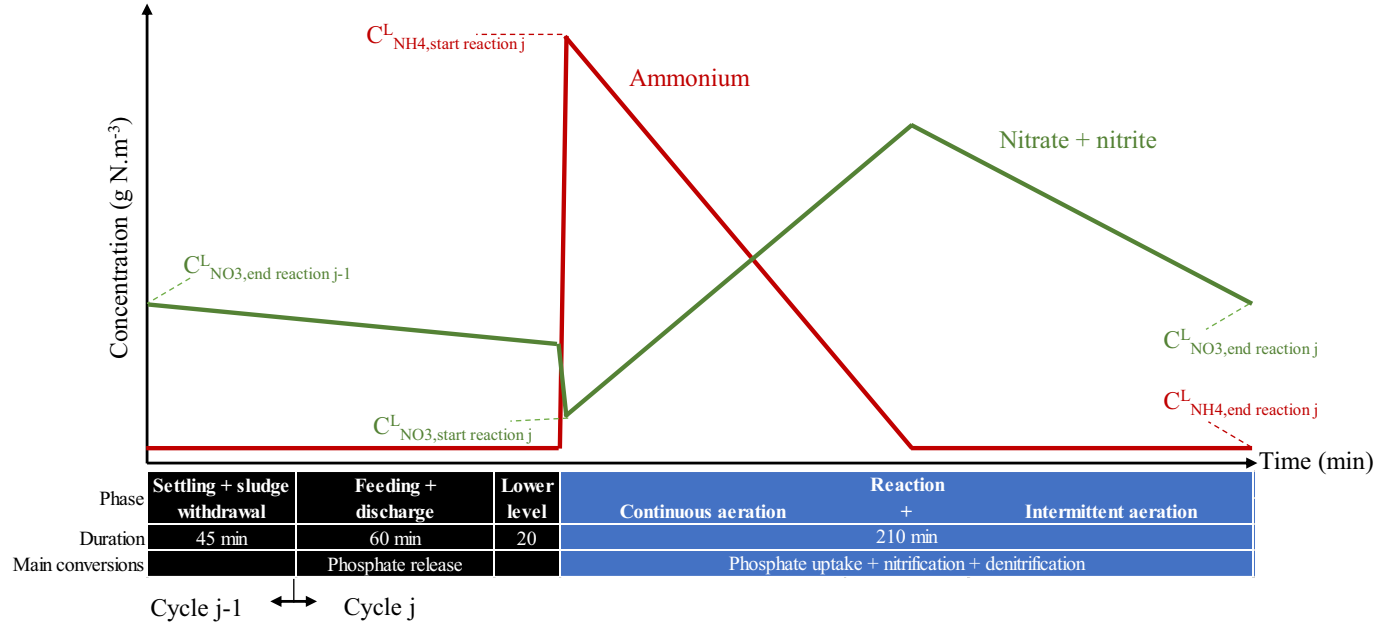

Fig. 3. Typical phase durations and ammonium and nitrate/nitrite concentration profiles measured at the top of the reactor during a dry weather cycle.

as the decrease of the total nitrogen mass, i.e. the sum of the ammonium and nitrate (Eq. (22)).

$$R^{L}_{NO3,reaction\ j} = \left[\left(C^{L}_{NH4} + C^{L}_{NO3}\right)_{start\ reaction\ j} - \left(C^{L}_{NH4} + C^{L}_{NO3}\right)_{end\ reaction\ j}\right] \cdot V^{L} \quad (22)$$

The residual denitrification during the remaining part of the cycle, $R^{L}_{NO3,residual\ j}$, was calculated as the decrease of the nitrate concentration between the end of the previous cycle's reaction phase and the nitrate concentration at the start of the current cycle's reaction phase, corrected for the output of nitrate via the effluent between these two moments (Eq. (23)).

$$R^{L}_{NO3,residual\ j} = \left[C^{L}_{NO3,end\ reaction\ j-1} - C^{L}_{NO3,start\ reaction\ j}\right] \cdot V^{L}_{in} - \sum_{end\ reaction\ j-1}^{start\ reaction\ j} C^{L}_{NO3}(t) \cdot Q^{L}_{in}(t) \cdot \Delta t \quad (23)$$

The cumulative masses of ammonium (Eq. (21)) and nitrate (Eqs. (22)–(23)) obtained over the whole monitoring period were compared to the mass of nitrified nitrogen (Eq. (19)) and the mass of denitrified nitrogen (Eq. (20)) to validate the accuracy of the mass balance calculations.

The amount of catabolized organics (aerobic and anoxic) during cycle j, $R^{L}_{COD,j}$, was calculated through a COD balance for this cycle (Eq. (24)), which states that the catabolized organics equal the absorbed oxygen $m^{G-L}_{O2,j}$ (derived from integration of Eq. (6)) minus the theoretical oxygen consumption for the removal of ammonium $R^{L}_{NH4,j}$ (Eq. (21)), plus the COD catabolized via denitrification (Eq. (22)).

$$R^{L}_{COD,j} = m^{G-L}_{O2,j} - 4.57\ g\ O_2 \cdot g\ N^{-1} \cdot R^{L}_{NH4,j} + 2.86\ g\ COD \cdot N^{-1} \cdot R^{L}_{NO3,j} \quad (24)$$

As this calculation relies on the removal of ammonium (Eq. (21)) and nitrate (Eqs. (22)–(23)) per cycle, which can only be observed from on-line measurements for sequentially operated reactors, also Eq. (24) is only valid for such reactors.

3. Results and discussion

3.1. Liquid-gas transfer rates

In this section, the dynamics of the liquid-gas transfer rates in the granular sludge reactor (Eq. (6); Fig. 4A) are analyzed for two cycles and related to the liquid phase concentrations (Fig. 4E), influent flow rate and air flow rate (Fig. 4D). Data for the other cycles are provided in Fig. S5.

The oxygen absorption and carbon dioxide emission rate showed comparable cyclic trends (Fig. 4A). At the start of the reaction phase, during continuous aeration, a short steep increase was first seen, followed by a prolonged slower increase. Later in the reaction phase, during the intermittent aeration, short steep increases were again seen during the aerated periods, but the rate did not reach the same levels as during the continuous aeration, due to the lower air flow rate used (Fig. 4D). The close relationship between both gasses' transfer rates can be understood by the coupling of oxygen consumption and carbon dioxide production via the oxidation of organics and nitrification. During the catabolic oxidation of typical organics, with an elemental composition $CH_{1.6}O_{0.3}$ (Hellinga et al., 1996), 1.1 g CO_2 is produced per gram of O_2 consumed (Eq. (25)).

$$CH_{1.6}O_{0.3} + 1.25\ O_2 \rightarrow CO_2 + 0.8\ H_2O \quad (25)$$

The oxygen consumption via nitrification is also indirectly coupled with the production of carbon dioxide. Even though some carbon dioxide is consumed for autotrophic biomass synthesis, the protons produced during nitrification (Eq. (26)) shift the chemical carbon dioxide/bicarbonate equilibrium towards carbon dioxide, causing extra stripping (Eq. (27)).

$$NH_4^{+} + 2\ O_2 \rightarrow NO_3^{-} + H_2O + 2H^{+} \quad (26)$$

$$HCO_{3-} + H^{+} \rightleftharpoons CO_2 + H_2O \quad (27)$$

The relationship between carbon dioxide emission and oxygen absorption rates is not perfectly linear (Fig. S6). This is partly explained by the pH dependency of the amount of carbon dioxide that is chemically produced per gram of nitrified ammonium (Weissenbacher et al., 2007; Spérandio and Paul, 1997). Secondly, after unaerated periods, the start-up of aeration was associated with a relatively higher carbon dioxide emission rate compared to the oxygen absorption rate, while continued aeration was associated with a relative decrease of the carbon dioxide emission rate compared to the oxygen absorption rate (Fig. 4A). This can be explained by accumulation of carbon dioxide during the unaerated phases, which led to an oversaturation and subsequent stripping when aeration was turned on. More precisely, during the feeding phase, carbon dioxide entered via the influent (Jin et al., 2015) and it was produced during the conversion of readily degradable COD to intracellular storage polymers (Smolders et al., 1995) and some denitrification (van Dijk et al., 2018). During the non-aerated periods in the reaction phase, accumulation of carbon dioxide occurred due to oxidation of substrates via denitrification.

It should be noted that the initial steep increase in the liquid-gas transfer rates immediately after non-aerated periods was partly due to the response time of the off-gas measurements. The residence time of the off-gas in the floating hood was around 4 min when the aeration rate was 8 $m^3 \cdot min^{-1}$ (Fig. S7). This did not lead to a pure time delay that could be easily corrected as in Eq. (5), because mixing occurred between the new off-gas and gas already present in the hood. Assuming a perfectly mixed gas, a step change in the actual off-gas oxygen concentration would lead to a measurement signal that reaches 95% of the actual value in three times the residence time (Hendricks, 2006), which amounts to a 12 min delay when the aeration rate was 8 $m^3 \cdot min^{-1}$. All liquid-gas transfer rates and derived variables during these periods were thus distorted and were therefore interpreted with care. Yet, when the aeration rate was maximal (16 $m^3 \cdot min^{-1}$), the residence time in the hood was reduced to 2 min (meaning ±6 min delay), causing only minimal distortion. As the increase in the oxygen absorption rate after feeding lasted much longer than the delay of 6 min, the prolonged slower increase was not a measurement artefact.

Methane emissions occurred mainly upon the start of aeration, immediately after feeding (Fig. 4A), which can be explained by dissolved methane entering via the influent (Foley et al., 2009). Note that the peaks in the methane emission rate were also distorted by the residence time in the floating hood due to the initial slow aeration rate. After reaching a peak, methane emissions decreased almost exponentially, which is typical for a stripping profile (Mampaey et al., 2015). Nitrous oxide emissions also peaked closely after the feeding phases (Fig. 4A). Even though these measurements do not allow exact identification of the formation pathway, there are three reasons to believe that it was formed during the feeding phases via heterotrophic or nitrifier denitrification of the residual nitrate/nitrite from the previous cycles (Kampschreur et al., 2009). First, the lag of the peak corresponded well with the 12 min delay in the measurements. Secondly, cycles where little nitrate/nitrite was left during the previous cycle resulted in a much smaller initial peak (Fig. S5), indicating that nitrate/nitrite reduction was indeed the source. Finally, a pilot-scale study also indicated nitrous oxide production during feeding when nitrate/nitrite was left from the previous cycle (Velho et al., 2017). A second nitrous oxide

emission peak always occurred after some time with high aeration (Fig. 4A). The high nitrification rates at this moment and the limited simultaneous denitrification with this specific applied control strategy (Fig. 4E) suggest that this nitrous oxide was formed during nitrification, via the hydroxylamine pathway (Sabba et al., 2018). A lab-scale study showed that nitrification can indeed be a source of nitrous oxide in aerobic granular sludge reactors (Gao et al., 2016). In the period where most of the denitrification occurred, i.e. during intermittent aeration, no significant emissions were observed. This indicates that the N_2O production was balanced by its consumption (Conthe et al., 2019).

Even though liquid-gas transfer rates can also be calculated from off-gas analyses (Eq. (6)) for continuous systems, this section illustrated how changes in the transfer rates can be more easily related to processes in the liquid phase with sequential operation. This is because these

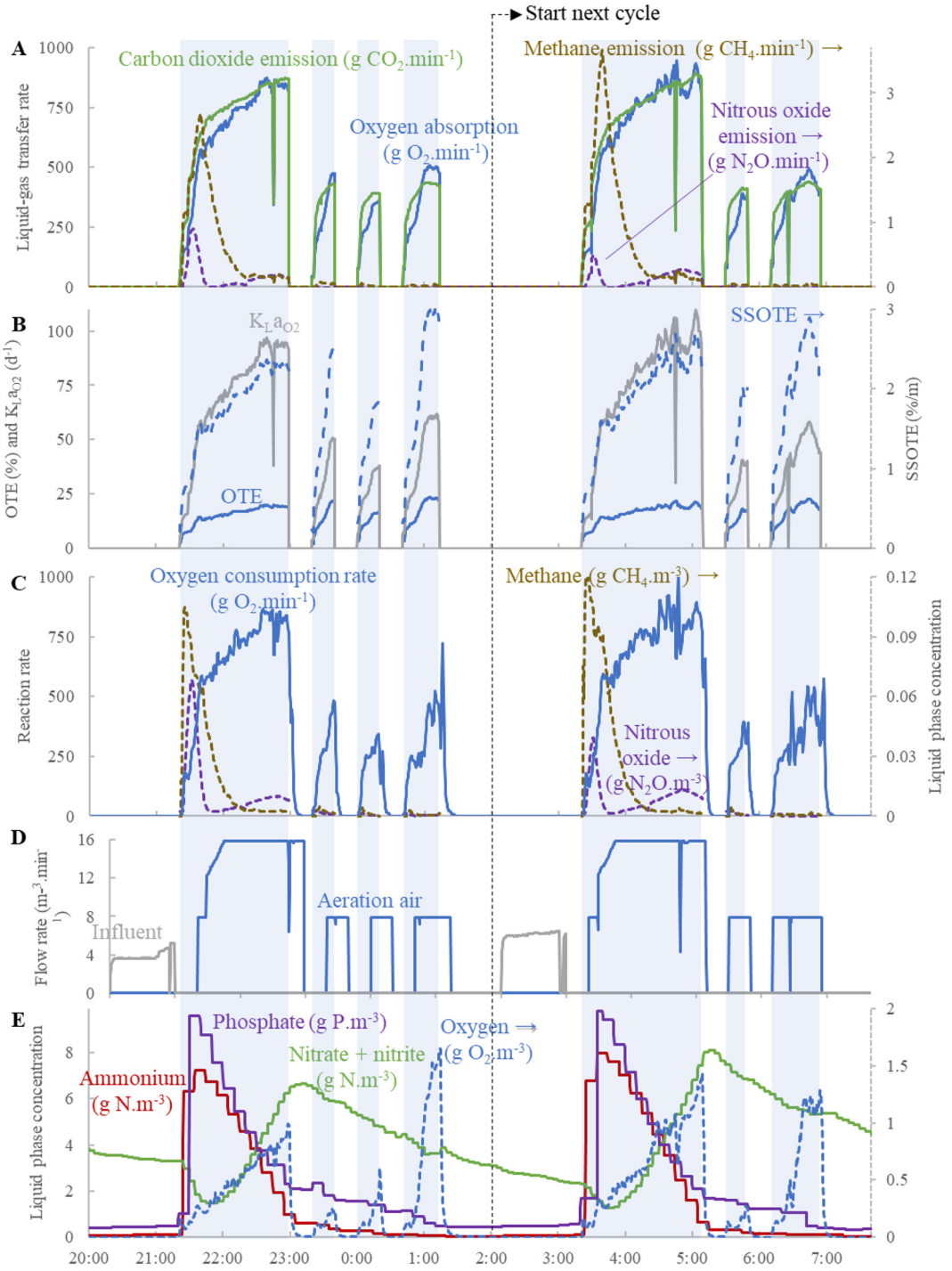

Fig. 4. On-line measurement results of two cycles of the aerobic granular sludge reactor in the night of 2 August to 3 August 2017, fed with 230 and 341 m^3 of influent respectively, corresponding to 18 and 27% exchange of the reactor volume. Aerated phases are indicated with a blue shade in all subfigures and values of dashed lines are indicated on the secondary y-axis. (A) Liquid-gas transfer rates of oxygen, carbon-dioxide, methane and nitrous oxide. (B) Aeration characteristics: (specific standard) oxygen transfer efficiency and liquid-gas mass transfer coefficient. (C) Consumption rate of oxygen and liquid phase concentrations of methane and nitrous oxide, derived from the off-gas composition. (D) Influent flow rate and air flow rate into the reactor. (E) Liquid phase concentration of ammonium, nitrate, phosphate and oxygen. (For interpretation of the references to colour in this figure legend, the reader is referred to the web version of this article.)

changes can be related to the phase in the cycle, such as the start of aeration, the end of nitrification or re-aeration after a non-aerated period.

3.2. Aeration characteristics

As in most full-scale off-gas studies (Table 1), aeration characteristics were derived from the oxygen absorption rate and liquid phase concentration (Eqs. (7), (12) and (13)), but the sequential operation of aerobic granular sludge reactors leads to pronounced cyclic dynamics (Fig. 4B). The liquid-gas transfer coefficient K_La_{O2} and (standard) oxygen transfer efficiency all gradually increased after feeding. This gradual improvement is likely due to slow degradation of pollutants with affinity for the liquid/gas interface which hinder mass transfer at the bubble surface. Surfactants, such as fatty acids and detergents, are known to be present in wastewater and have this effect (Rosso et al., 2006). The gradual improvement was less pronounced in cycles with a small volume of influent added (Fig. S5), which is in line with the hypothesis of surfactants degradation. A similar gradual improvement has been observed within cycles of other sequentially operated reactors with granular (Cecconi et al., 2019) and flocculent sludge (Ronner-Holm et al., 2006) and along the flow direction in continuously fed and aerated systems (Amerlinck et al., 2016; Redmon et al., 1983). The variation of the K_La_{O2} under process conditions should be considered when designing the aeration equipment of new reactors.

The maximum K_La_{O2} under process conditions (sometimes called αFK_La_{O2}) during the monitoring period was 110 d^{-1} (Fig. S5), which corresponds to 108 d^{-1} at the standard temperature of 20 °C (Redmon et al., 1983). An earlier independent measurement on the same reactor via the dynamic method, which is based on dissolved oxygen measurements only (Garcia-Ochoa and Gomez, 2009), found a value of 131 d^{-1} under clean water conditions. The lower value (18%) measured under process conditions with the off-gas method can be explained by residual surfactants, diffuser fouling and the use of a Henry coefficient for pure water (Eq. (8)) (Baquero-Rodriguez et al., 2018). The specific standard oxygen transfer efficiency reached cycle maxima between 2.5 and 3.3%·m^{-1} during the complete monitoring campaign (Fig. S5), which lies close to the range of 2.9–3.7%·m^{-1} observed in a pilot-scale granular sludge reactor (Cecconi et al., 2019). The aeration efficiency under process conditions (Eq. (14)) was 1.53 kg O_2·kWh^{-1} on average, which lies in the typical range of 0.7–2.6 kg O_2·kWh^{-1} for fine pore diffusers in clean water (Henze et al., 2008). As aeration characteristics are affected by salinity, surfactants, fouling, biomass concentration, diffuser type, reactor operation, aggregate size (granules vs flocs) (Cecconi et al., 2019) etc., the individual contribution of each of these factors to the measured values cannot be disclosed without dedicated experiments (Baquero-Rodriguez et al., 2018).

Table 2
N_2O emission factors reported in literature.

N_2O (% of N load)	Wastewater type (x g COD·m^{-3}; y g NH_4^+-N·m^{-3})	Reference
Full-scale aerobic granular sludge reactor		
0.062	Municipal	This study
0.69	Municipal	de Bruin et al. (2013)
Lab-scale aerobic granular sludge reactors		
52.5	Potato	Dobbeleers et al. (2017)
0.7–12.9	Synthetic (400; 50)	Lochmatter et al. (2014)
7.0–22	Synthetic (300; 45)	Zhang et al. (2015)
7–9	Synthetic (400; 50)	Lochmatter et al. (2013)
2.8	Municipal	Guimarães et al. (2017)
2.72	Synthetic (800; 100)	Gao et al. (2016)
1.6	Municipal	Velho et al. (2017)
0.6	Synthetic (1047; 63)	Kong et al. (2013)
0.12	Slaughterhouse	Dobbeleers et al. (2018)
Full-scale activated sludge reactors		
0–11.2	Municipal	Foley et al. (2011)

3.3. Liquid phase concentrations

The dissolved methane and nitrous oxide concentrations were estimated (Fig. 4C) from their measured liquid-gas transfer rates and respective transfer coefficients K_La_i (Eq. (15)), derived from the K_La_{O2} at every moment (Eq. (11)). Even though the slow aeration at the beginning of the aeration phases distorted the estimated methane concentrations (as explained in Section 3.1), the values provide an indication of the influent methane concentration. Considering the peaks of the methane concentration and the added volume of influent per cycle, the average methane concentration in the influent was 0.5% of the influent COD (0.7 g CH_4·m^{-3}), which is close to the 0.6% reported by Liu et al. (2014) and lower than the 1% reported by Daelman et al. (2012). This low value can be explained by differences in the sewer system and absence of an anaerobic digester (Foley et al., 2009). For nitrous oxide, the liquid phase concentrations during the second peak were more accurately estimated than during the first peak, as the aeration rate was faster here, limiting the measurement artefact. The new procedure demonstrated here to estimate dissolved concentrations from off-gas is applicable to both sequential and continuous reactors. It also requires less assumptions and no model fitting, which makes it easier to automate than previously developed methods (Weissenbacher et al., 2007; Mampaey et al., 2015; Castro-Barros et al., 2015). The same procedure can be used to estimate the concentration of other volatile substances, such as nitric oxide. A validation of the method with an independent measurement technique is still required.

3.4. Conversion rates

The oxygen consumption rate (often called oxygen uptake rate or OUR) could be estimated from the absorption rate and liquid phase concentration of oxygen (Eq. (16)) thanks to the sequential reactor operation (Fig. 1). The observed trend (Fig. 4C) is the result of oxygen consumption via nitrification, oxidation of soluble organics and oxidation of intracellular storage polymers. The rates of these processes depend on the concentration of their respective substrates. For example, the nitrification rate (r_{NH4}) in an aerobic granular sludge reactor increases with increasing dissolved ammonium (S_{NH4}) and oxygen concentrations (S_{O2}) according to Monod kinetics with apparent half-saturation coefficients $K_{NH4,app}$ and $K_{O2,app}$ and maximum rate r_{max} (Baeten et al., 2018).

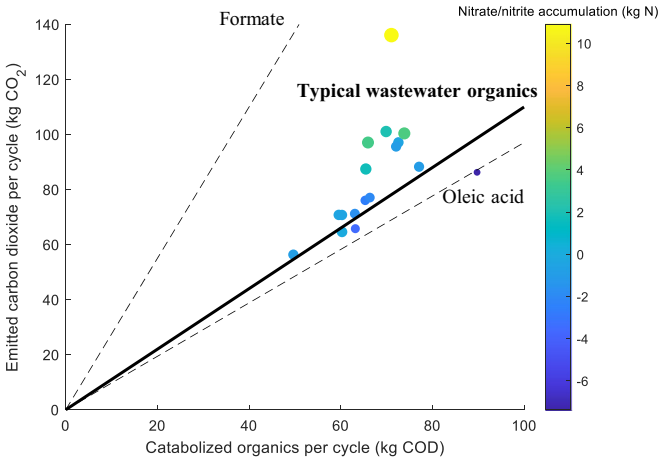

Fig. 5. The net carbon dioxide emitted versus the amount of catabolized COD, for each cycle in the monitoring campaign. The lines indicate the theoretical carbon dioxide production during oxidation of typical wastewater organics, formate and oleic acid. The net nitrate accumulation in a cycle is indicated with the colour and size of the marker. (For interpretation of the references to colour in this figure legend, the reader is referred to the web version of this article.)

$$r = r_{max} \frac{S_{NH4}}{K_{NH4,app} + S_{NH4}} \frac{S_{O2}}{K_{O2,app} + S_{O2}} \quad (28)$$

Immediately after feeding, the liquid phase oxygen concentration gradually increased from 0 to above 1 $g \cdot m^{-3}$ (Fig. 4E), so the oxygen limitation of the aerobic conversions decreased and the oxygen consumption rate increased. Later in the cycle, during the intermittent aeration, the oxygen concentration reached similar and even higher values (up to 1.7 $g \cdot m^{-3}$), but the oxygen consumption rate was lower, because other substrates became limiting instead, e.g. biodegradable COD, internal storage polymers and especially ammonium. It is expected that continued aeration would lead to a clear inflection point when nitrification is complete, but this was not visible because the current control strategy stopped the aeration at exactly this moment. In reactors without this control strategy, a bending point in the oxygen consumption rate could be used to detect the completion of nitrification.

3.5. Pollutant emissions (methane and N_2O)

Where the previous sections focused on dynamics within cycles, the total amounts transferred to or from the liquid phase over one or more cycles are discussed below.

During the 4.5 days monitoring campaign, the methane emission factor was 0.7 mg CH_4 per gram influent COD. This lies just below the range 0.8–12 found in other full-scale plants, without granular sludge (Daelman et al., 2012). The nitrous oxide emission factor was 0.06% of the nitrogen load (0.08% of the removed ammonium). This is the lowest value reported for an aerobic granular sludge reactor, but it is also only the second full-scale value (Table 2). The broad observed ranges of emission factors from aerobic granular sludge, activated sludge and biofilm reactors show that they are not simply a function of the degree of biomass aggregation, but that the design and operating conditions play a crucial role (Kampschreur et al., 2009; Wan et al., 2019; Todt and Dorsch, 2016). For example, nitrous oxide emissions are often correlated with the ammonium load for both granular and activated sludge reactors (Gao et al., 2016; Daelman et al., 2015; Chandran et al., 2011). This was also found during the short-term campaign in this study ($r = 0.84$). The goal of this study was not to determine a general emission factor to estimate carbon footprints of aerobic granular sludge reactors, as long-term monitoring campaigns on multiple plants are required for this (Daelman et al., 2013b).

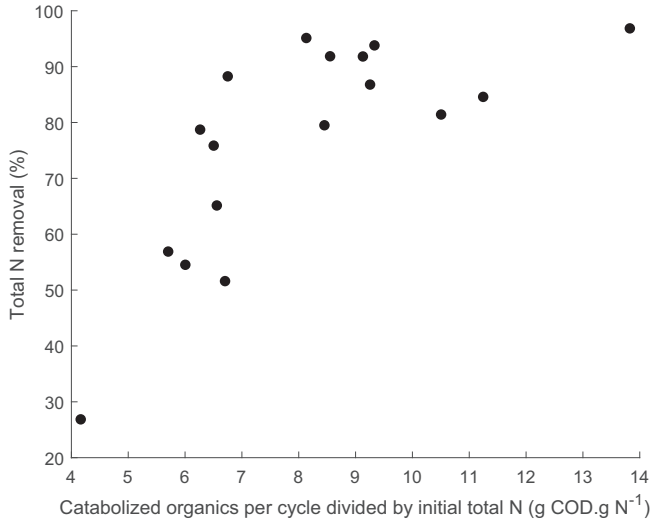

Fig. 6. The total nitrogen removal versus the amount of catabolized COD, for each cycle in the monitoring campaign.

3.6. Wastewater composition

To get an indication of the TOC/COD ratio, the cumulative carbon dioxide emission was plotted against the amount of catabolized COD derived from the total oxygen absorption and liquid phase sensors (Eq. (24)) for each cycle of the monitoring campaign (Fig. 5). The carbon dioxide emissions corresponded well with the theoretically expected value of 1.1 g CO_2 per gram COD (Eq. (25)) in cycles with a near zero net nitrate/nitrite accumulation. A high net nitrate/nitrite accumulation was associated with higher carbon dioxide emissions than expected from COD oxidation only. This can be explained by the additional carbon dioxide production that occurs during nitrification (Eq. (26)) by shifting the bicarbonate equilibrium to the right (Eq. (27)) (Henze et al., 2008). In contrast, there was an unexpectedly low carbon dioxide emission during one cycle with a strongly negative net nitrate/nitrite accumulation. The negative accumulation was caused by nitrate/nitrite remaining from the previous cycle (Fig. S5), which allowed more denitrification than nitrification. The extra denitrification caused proton consumption and therefore shifted the bicarbonate equilibrium to the left.

To get an idea of the sensitivity of the carbon dioxide emission to variations in the influent organics composition, the theoretically expected values for oxidation of oleic acid ($C_{18}H_{34}O_2$) and formate (CH_2O_2) were included in Fig. 5. This shows that off-gas analysis could give an indication of the carbon content of wastewater organics without calibration of an extensive bioconversion model (Leu et al., 2010): a batch with strongly deviating TOC/COD ratio could be noticed for example as a blue dot which lies far away from the bold line. By producing this graph with a long-term dataset, deviations from typical cycles could be detected for a specific plant. This diagnostic graph (Fig. 5) could only be created based on on-line measurements in the reactor (ammonium and nitrate) and off-gas (oxygen and carbon dioxide) due to the sequential reactor operation, because the measurements directly reflect the conversions during the reaction phases, without interference by mass flows via the influent or effluent (Fig. 1).

To get an indication of the COD/N ratio present at the start of each aeration phase, the catabolized COD (Eq. (24)) was divided by the total nitrogen present at the start of each aeration phase, which was calculated from the on-line measured liquid phase ammonium plus nitrate. The total nitrogen removal efficiency during each cycle was also derived from liquid phase measurements of ammonium and nitrate (Eq. (22) plus Eq. (23)). A higher COD/N ratio was associated with a better total nitrogen removal (Fig. 6). This is expected because organics are required for denitrification (Henze et al., 2008). Similar to Fig. 5, also this type of diagnostic graph (Fig. 6) was only possible thanks to the sequential operation of the reactor: the on-line liquid phase measurements of ammonium and nitrate directly indicate the nitrogen removal during the separate reaction phase and combined with the off-gas oxygen measurements, the catabolized COD can be estimated (Fig. 1).

3.7. Sludge production

The off-gas measurements were used to close the mass balance of oxygen, COD, nitrogen and nitrate and as such estimate several unmeasured variables (Eqs. (17)–(20)), shown in Fig. 7. The ammonium and nitrate removal could be derived directly from the liquid phase measurements (Eqs. (21)–(23)) and were 119 and 111 kg N respectively, which closely matched the total nitrified and denitrified nitrogen derived from the mass balances of 111 and 103 kg N respectively. The small difference (8%) has several potential causes. First of all, the delay in the off-gas analysis led to an underestimation of the absorbed oxygen. Secondly, assumptions were made in the mass balance calculations, e.g. historical average influent and effluent concentrations were used and no nitrification and denitrification via nitrite was considered. Finally, the ammonium and nitrate removal derived from the liquid phase measurements do not purely reflect nitrification and denitrification, since

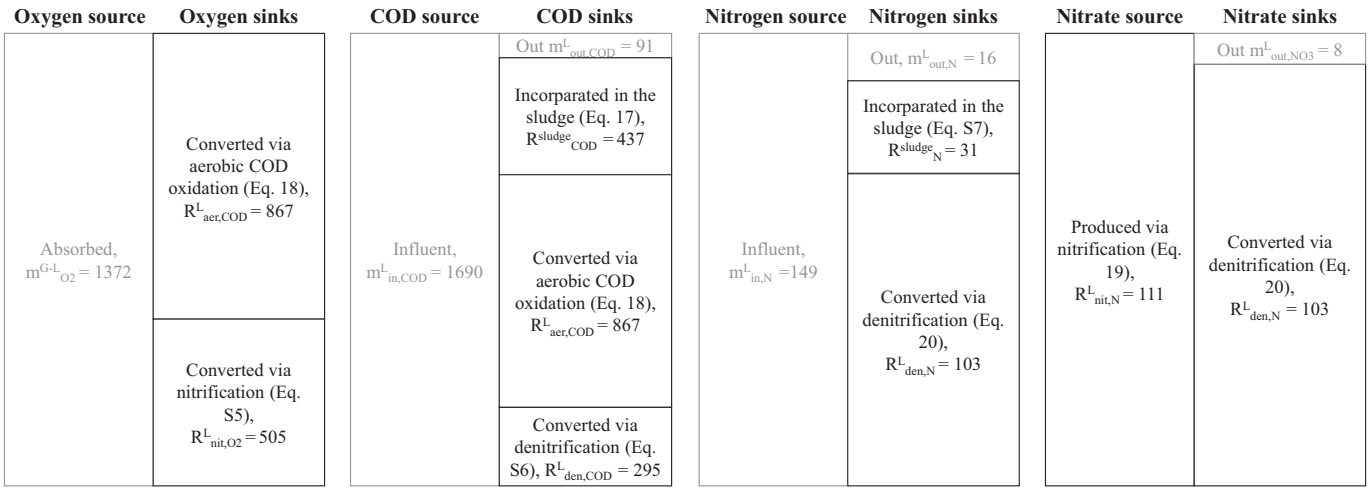

Fig. 7. Mass balances of oxygen (kg O_2), COD (kg COD), nitrogen (kg N) and nitrate (kg N) over the monitoring period. The black variables were calculated via the mass balance equations (Eqs. (17)–(20)), while grey variables were measured.

uptake of ammonium for growth, release during ammonification and absorption and desorption onto the biomass (Bassin et al., 2011) occur simultaneously. Still, the similarity of the independently derived variables gives confidence in the mass balance calculations.

For continuously operated reactors, mass balances can be closed using off-gas analyses as well, but there may be more added value for sequentially operated granular sludge reactors, because the sludge production can be quantified in this manner (437 kg COD according to Fig. 7). Conventional methods of measuring sludge production are complicated due to the rapidly fluctuating concentration in the waste stream in this case. Dividing the sludge production by the total COD removal (1690–91 kg COD) gives an observed yield of 0.27 g COD per gram of COD removed. This lies between the 0.2 reported for a lab-scale (Mosquera-Corral et al., 2005) and 0.34 g COD·g COD^{-1} reported for another full-scale aerobic granular sludge reactor (Pronk et al., 2015) (calculated assuming 1.48 g COD·g VSS^{-1} (Henze et al., 2008)). This variability of observed yields can be explained by different solids retention times and influent characteristics (Henze et al., 2008). A typical solids retention time in an aerobic granular sludge reactor is 10–30 days (Pronk et al., 2015), which corresponds to an apparent yield of active biomass in the range of 0.09–0.21 g COD·g COD^{-1}, using a typical intrinsic yield $Y_{intrinsic}$ of 0.625 g COD·g COD^{-1} and decay rate b of 0.2 d^{-1} (Henze et al., 2000) in Eq. (29) (Rosso and Stenstrom, 2005).

$$Y_{apparent} = \frac{Y_{intrinsic}}{1 + b \cdot SRT} \quad (29)$$

The observed yields found for the full-scale reactors were higher than this range of apparent yields because the estimated COD incorporation in the sludge also comprised influent particulate unbiodegradable COD.

3.8. Perspectives

As the processes inside the liquid phase are of primary concern during wastewater treatment, liquid phase measurements of ammonium, nitrate and phosphate are the most obvious variables for monitoring and control. Yet, for sequentially operated reactors, the low maintenance requirements and diversity of variables that can be derived with a single off-gas sampler may justify a place for off-gas analyzers as part of the typical instrumentation. Continuous off-gas measurements may not only be used to detect fouling and thus allows timely diffuser cleaning (Section 3.2). It could also be used to control the length of the phases, e.g. by using the oxygen consumption rate to detect when nitrification is nearly complete (Section 3.4). It allows to make a greenhouse gas emission inventory and find mitigation strategies (Sections 3.1, 3.3 and 3.5). Strongly abnormal (illegal) discharges could be detected and low nitrogen removal efficiencies may be diagnosed on the small time-scale of one cycle, which allows more timely action than 24-hour composite samples (Section 3.6). Furthermore, the start-up of a reactor may be tracked and the sludge transport and treatment requirements may be assessed by estimating the sludge production (Section 3.7). This work aimed to give an overview of the diversity of applications of off-gas analyses, but for use in practice, a floating hood with a smaller volume/area ratio is preferable to minimize the response time, which is more crucial in sequentially operated reactors given the fast changes of the transfer rates on a time scale of minutes (Section 3.1).

4. Conclusions

- Off-gas analyses have potential for monitoring and control of sequentially operated reactors because the absence of feeding and discharge during the reaction phases allows more representative sampling and simplifies the calculation of several variables.
- A single set-up for off-gas sampling and analysis allows the derivation of multiple variables: liquid-gas transfer rates, aeration characteristics (e.g. K_La_{O2}), liquid phase concentrations of emitted substances and conversion rates within every cycle and also pollutant emissions, influent characteristics (TOC/COD and COD/N ratio) and sludge production over one or more cycles.
- Application to a full-scale aerobic granular sludge reactor led to novel process insights: a gradual improvement of the aeration characteristics was observed within cycles due surfactants degradation, carbon dioxide and oxygen transfer rates were correlated due to the coupling of carbon dioxide production and oxygen consumption, methane showed a stripping profile immediately after feeding and nitrous oxide often showed both a stripping profile immediately after feeding and a peak coinciding with high nitrification rates.

CRediT authorship contribution statement

Janis E. Baeten: Conceptualization, Methodology, Software, Investigation, Writing – original draft, Writing – review & editing, Visualization. **Edward J.H. van Dijk:** Conceptualization, Methodology, Software, Investigation, Writing – review & editing. **Mario Pronk:** Conceptualization, Methodology, Investigation, Writing – review & editing. **Mark C.M. van Loosdrecht:** Conceptualization, Writing – review & editing. **Eveline**

I.P. Volcke: Conceptualization, Methodology, Validation, Writing – review & editing.

Declaration of competing interest

The authors declare the following financial interests/personal relationships which may be considered as potential competing interests: Two of the authors are employed by the company that markets the technology that is under study.

Acknowledgements

This work was supported by the Research Foundation - Flanders (FWO Fellowship Janis Baeten). We are grateful to Royal HaskoningDHV and the water board Rijn en IJssel for the collaboration and for sharing the data. We thank Suellen Espindola and Udo van Dongen for their technical assistance with the monitoring campaign.

Appendix A. Supplementary data

Supplementary data to this article can be found online at https://doi.org/10.1016/j.scitotenv.2021.147651.

References

Amerlinck, Y., Bellandi, G., Amaral, A., Weijers, S., Nopens, I., 2016. Water Sci. Technol. 74, 203–211.
ASCE, 1997. Standard Guidelines for In-Process Oxygen Transfer Testing, New York.
Aviles, A.B.L., Velazquez, F.D., Riquelme, M.L.P. Del, 2020. Water 12.
Baeten, J.E., van Loosdrecht, M.C.M., Volcke, E.I.P., 2018. Water Res. 146, 134–145.
Baeten, J.E., van Loosdrecht, M.C.M., Volcke, E.I.P., 2020. Water Res. 178, 115844.
Baquero-Rodriguez, G.A., Lara-Borrero, J.A., Nolasco, D., Rosso, D., 2018. Water Environ. Res. 90, 431–441.
Bassin, J.P., Pronk, M., Kraan, R., Kleerebezem, R., van Loosdrecht, M.C.M., 2011. Water Res. 45, 5257–5265.
Bellandi, G., Porro, J., Senesi, E., Caretti, C., Caffaz, S., Weijers, S., Nopens, I., Gori, R., 2018. Water Sci. Technol. 77, 880–890.
Butler, M.D., Wang, Y.Y., Cartmell, E., Stephenson, T., 2009. Water Res. 43, 1265–1272.
Caivano, M., Bellandi, G., Mancini, I.M., Masi, S., Brienza, R., Panariello, S., Gori, R., Caniani, D., 2017. Environ. Technol. 38, 629–638.
Caniani, D., Caivano, M., Pascale, R., Bianco, G., Mancini, I.M., Masi, S., Mazzone, G., Firouzian, M., Rosso, D., 2019. Sci. Total Environ. 648, 1130–1140.
Castro-Barros, C., Daelman, M., Mampaey, K., van Loosdrecht, M.C.M., Volcke, E.I.P., 2015. Water Res. 68, 793–803.
Cecconi, F., Garrido-Baserba, M., Eschborn, R., Damerel, J., Rosso, D., 2019. Environ. Sci. Water Res. Technol. 6, 679–690.
Chandran, K., Stein, L.Y., Klotz, M.G., van Loosdrecht, M.C.M., 2011. Biochem. Soc. Trans. 39, 1832–1837.
Chiesa, S.C., Rieth, M.G., Ching, T., 1990. J. Environ. Eng. ASCE 116, 472–486.
Conthe, M., Lycus, P., Arntzen, M.O., da Silva, A.R., Frostegard, A., Bakken, L.R., Kleerebezem, R., van Loosdrecht, M.C.M., 2019. Water Res. 151, 381–387.
Daelman, M.R.J., van Voorthuizen, E.M., van Dongen, U.G.J.M., Volcke, E.I.P., van Loosdrecht, M.C.M., 2012. Water Res. 46, 3657–3670.
Daelman, M.R.J., van Voorthuizen, E.M., van Dongen, U.G.J.M., Volcke, E.I.P., van Loosdrecht, M.C.M., 2013a. Water Sci. Technol. 67, 2350–2355.
Daelman, M.R.J., Baets, B. De, van Loosdrecht, M.C.M., Volcke, E.I.P., 2013b. Water Res. 47, 3120–3130.
Daelman, M.R.J., van Voorthuizen, E.M., van Dongen, U.G.J.M., Volcke, E.I.P., van Loosdrecht, M.C.M., 2015. Sci. Total Environ. 536, 1–11.
de Bruin, L.M.M., Bruin, B. de, Roest, H. van der, Bentem, A. van, Berkhof, D., van Dijk, E.J.H., Gool, H. van, Kraan, R., Krijgsman, J., Kuij, R. van der, van Loosdrecht, M.C.M., Meinema, K., Miska, V., Pronk, M., Verschoor, J., Winkler, M., 2013. Nereda praktijkonderzoeken 2010–2012. STOWA, Amersfoort.
Dobbeleers, T., Daens, D., Miele, S., D'aes, J., Caluwé, M., Geuens, L., Dries, J., 2017. Bioresour. Technol. 226, 211–219.
Dobbeleers, T., Caluwe, M., Daens, D., Geuens, L., Dries, J., 2018. J. Chem. Technol. Biotechnol. 93, 569–576.
Foley, J., Yuan, Z.G., Lant, P., 2009. Water Sci. Technol. 60, 2963–2971.
Foley, J., Yuan, Z., Senante, E., Chandran, K., Willis, J., van Loosdrecht, M.C.M., van Voorthuizen, E.M., 2011. N2O and CH4 Emission From Wastewater Collection and Treatment Systems - State of the Science Report. Global Water Research Coalition, London, UK.
Gao, M., Yang, S., Wang, M., Wang, X.-H., 2016. J. Biosci. Bioeng. 122, 601–605.
Gapes, D., Keller, J., 2001. Biotechnol. Bioeng. 76, 361–375.
Gapes, D., Pratt, S., Yuan, Z.G., Keller, J., 2003. Water Res. 37, 2678–2690.
Garcia-Ochoa, F., Gomez, E., 2009. Biotechnol. Adv. 27, 153–176.
Gillot, S., Heduit, A., 2000. Water Res. 34, 1756–1762.
Gillot, S., Heduit, A., 2008. Water Sci. Technol. 57, 1265–1269.
Gillot, S., Capela-Marsal, S., Roustan, M., Héduit, A., 2005a. Water Res. 39, 1379–1387.
Gillot, S., Kies, F., Amiel, C., Roustan, M., Héduit, A., 2005b. Chem. Eng. Sci. 60, 6336–6345.
Groves, K.P., Daigger, G.T., Simpkin, T.J., Redmon, D.T., Ewing, L., 1992. Water Environ. Res. 64, 691–698.
Guimarães, L.B., Mezzari, M.P., Daudt, G.C., da Costa, R.H., 2017. J. Chem. Technol. Biotechnol. 92, 1756–1765.
Hellinga, C., Vanrolleghem, P., van Loosdrecht, M.C.M., Heijnen, J.J., 1996. Water Sci. Technol. 33, 13–23.
Hendricks, D.W., 2006. Water Treatment Unit Processes: Physical and Chemical. Taylor & Francis, Boca Raton, Florida, USA.
Henze, M., Gujer, W., Mino, T., van Loosdrecht, M.C.M., 2000. Activated Sludge Models ASM1, ASM2, ASM2d and ASM3. IWA Publishing, London, UK.
Henze, M., van Loosdrecht, M.C.M., Ekama, G.A., Brdjanovic, D., 2008. Biological Wastewater Treatment: Principles, Modelling and Design. IWA Publishing, London, UK.
heyder, B. De, Vanrolleghem, P., Langenhove, H. Van, Verstraete, W., 1997. Biotechnol. Bioeng. 55, 511–519.
Jin, P., Wang, B., Jiao, D., Sun, G., Wang, B., Wang, X.C., 2015. Water Res. 84, 112–119.
Kampschreur, M.J., Temmink, H., Kleerebezem, R., Jetten, M.S.M., van Loosdrecht, M.C.M., 2009. Water Res. 43, 4093–4103.
Keller, J., Yuan, Z., 2002. Water Sci. Technol. 45, 219–228.
Kent, T.R., Bott, C.B., Wang, Z.-W., 2018. Biotechnol. Adv. 36, 1139–1166.
Kong, Q., Zhang, J., Ngo, H.H., Ni, S., Fu, R., Guo, W., Guo, N., Tian, L., 2013. Int. Biodeterior. Biodegradation 85, 533–538.
Le, Q.H., Verheijen, P.J.T., Mampaey, K.E., van Loosdrecht, M.C.M., Volcke, E.I.P., 2016. IFAC-PapersOnLine 49, 1139–1144.
Leu, S.Y., Rosso, D., Larson, L.E., Stenstrom, M.K., 2009. Water Environ. Res. 81, 2471–2481.
Leu, S.-Y., Libra, J.A., Stenstrom, M.K., 2010. Water Res. 44, 3434–3444.
Lindblom, E., Arnell, M., Flores-Alsina, X., Stenstrom, F., Gustavsson, D.J.I., Yang, J., Jeppsson, U., 2016. Water Sci. Technol. 73, 798–806.
Liu, Y., Cheng, X., Lun, X., Sun, D., 2014. J. Environ. Sci. 26, 224–230.
Lochmatter, S., Gonzalez-Gil, G., Holliger, C., 2013. Water Res. 47, 6187–6197.
Lochmatter, S., Maillard, J., Holliger, C., 2014. Int. J. Environ. Res. Public Health 11, 6955–6978.
Makinia, J., Wells, S.A., 2000. Water Res. 34, 3987–3996.
Mampaey, K.E., van Dongen, U.G.J.M., van Loosdrecht, M.C.M., Volcke, E.I.P., 2015. Environ. Technol. 36, 1680–1690.
Mampaey, K.E., Kreuk, M.K. De, Dongen, U. van, van Loosdrecht, M.C.M., Volcke, E.I.P., 2016. Water Res. 88, 575–585.
Mears, L., Stocks, S.M., Sin, G., Gernaey, K.V., 2017. J. Biotechnol. 245, 34–46.
Meijer, S.C.F., van Loosdrecht, M.C.M., Heijnen, J.J., 2001. Water Res. 35, 2711–2723.
Mosquera-Corral, A., de Kreuk, M.K., Heijnen, J.J., van Loosdrecht, M.C.M., 2005. Water Res. 39, 2676–2686.
Mueller, J.A., Kim, Y.K., Krupa, J.J., Shkreli, F., Nasr, S., Fitzpatrick, B., 2000. J. Environ. Eng. ASCE 126, 549–555.
Ni, B.J., Xie, W.M., Liu, S.G., Yu, H.Q., Wang, Y.Z., Gan, W., Dai, X.L., 2009. AIChE J. 55, 2186–2196.
Pronk, M., de Kreuk, M.K., Bruin, B. de, Kamminga, P., Kleerebezem, R., van Loosdrecht, M.C.M., 2015. Water Res. 84, 207–217.
Pronk, M., Giesen, A., Thompson, A., Robertson, S., Loosdrecht, M. van, 2017. Water Pract. Technol. 12, 987–996.
Racault, Y., Stricker, A.E., Husson, A., Gillot, S., 2011. Water Sci. Technol. 63, 2651–2657.
Redmon, D., Boyle, W.C., Ewing, L., 1983. J. Water Pollut. Control Fed. 55, 1338–1347.
Rieth, M.G., Chiesa, S.C., Polta, R.C., 1995. Water Environ. Res. 67, 781–787.
Ronner-Holm, S.G.E., Mennerich, A., Holm, N.C., 2006. Water Sci. Technol. 54, 71–80.
Rosso, D., Stenstrom, M.K., 2005. Water Res. 39, 3773–3780.
Rosso, D., Iranpour, R., Stenstrom, M.K., 2005. Water Environ. Res. 77, 266–273.
Rosso, D., Larson, L.E., Stenstrom, M.K., 2006. Water Sci. Technol. 54, 143–153.
Rosso, D., Lothman, S.E., Jeung, M.K., Pitt, P., Gellner, W.J., Stone, A.L., Howard, D., 2011. Water Res. 45, 5987–5996.
Sabba, F., Terada, A., Wells, G., Smets, B.F., Nerenberg, R., 2018. Appl. Microbiol. Biotechnol. 102, 9815–9829.
Sahlmann, C., Libra, J.A., Schuchardt, A., Wiesmann, U., Gnirss, R., 2004. Water Sci. Technol. 50, 61–68.
Sandberg, M., 2010. Water Sci. Technol. 62, 2364–2371.
Schuchardt, A., Libra, J.A., Sahlmann, C., Wiesmann, U., Gnirss, R., 2007. Environ. Technol. 28, 479–489.
Shiskowski, D.M., Mavinic, D.S., 2005. Environ. Technol. 26, 843–856.
Shriver, D.F., Drezdzon, M.A., 1986. The Manipulation of Air-Sensitive Compounds. 2 edn. Wiley, USA.
Smolders, G.J.F., Vandermeij, J., Vanloosdrecht, M.C.M., Heijnen, J.J., 1995. Biotechnol. Bioeng. 47, 277–287.
Sonnleitner, B., 2013. Adv. Biochem. Eng. Biotechnol. 132, 1–33.
Spanjers, H., Vanrolleghem, P., Olsson, G., Doldt, P., 1996. Water Sci. Technol. 34, 117–126.
Spérandio, M., Paul, E., 1997. Biotechnol. Bioeng. 53, 243–252.
Spinelli, M., Eusebi, A.L., Vasilaki, V., Katsou, E., Frison, N., Cingolani, D., Fatone, F., 2018. J. Clean. Prod. 190, 517–524.
Sree, U., Bauer, H., Fuerhacker, M., Ellinger, R., Schmidt, H., Puxbaum, H., 2000. Water Air Soil Pollut. 124, 177–186.
Todt, D., Dorsch, P., 2016. Rev. Environ. Sci. Biotechnol. 15, 355–378.
van Dijk, E.J.H., Pronk, M., van Loosdrecht, M.C.M., 2018. Water Res. 147, 50–59.
Vanrolleghem, P.A., Lee, D.S., 2003. Water Sci. Technol. 47, 1–34.

Vanrolleghem, P.A., Insel, G., Petersen, B., Sin, G., Pauw, D. De, Nopens, I., Dovermann, H., Weijers, S., Gernaey, K.V., 2003. Proc. Water Environ. Fed. 2003, 210–237.
Velho, V.F., Magnus, B.S., Daudt, G.C., Xavier, J.A., Guimaraes, L.B., Costa, R.H.R., 2017. Water Sci. Technol. 76, 3452–3460.
Wan, X., Baeten, J.E., Volcke, E.I.P., 2019. Biochem. Eng. J. 143, 24–33.
Weissenbacher, N., Lenz, K., Mahnik, S.N., Wett, B., Fuerhacker, M., 2007. Water Res. 41, 1587–1595.
Winter, P., Pearce, P., Colquhoun, K., 2012. J. Water Clim. Chang. 3, 95–109.
Wu, J., Xu, T., Yan, G., He, C., Zhou, G., 2015. J. Environ. Chem. Eng. 3, 2857–2865.
Yoong, E.T., Lant, P.A., Greenfield, P.F., 2000. Water Res. 34, 239–245.
Zhang, F., Li, P., Chen, M., Wu, J., Zhu, N., Wu, P., Chiang, P., Hu, Z., 2015. Chem. Eng. J. 280, 549–557.